An Ultradeep Multiband Very Large Array Survey of the Faint Radio Sky (COSMOS-XS): New Constraints on the Optically Dark Population

van der Vlugt, D.; Hodge, J. A.; Jin, S.; Algera, H. S. B.; Leslie, S. K.; Riechers, D. A.; Röttgering, H.; Smolčić, V.; Walter, F.

The Astrophysical Journal, 951:131 (9pp), 2023 July 10 https://doi.org/10.3847/1538-4357/acd549

An Ultradeep Multiband Very Large Array Survey of the Faint Radio Sky (COSMOS-XS): New Constraints on the Optically Dark Population

D. van der Vlugt[1], J. A. Hodge[1], S. Jin[2,3], H. S. B. Algera[4,5], S. K. Leslie[1], D. A. Riechers[6], H. Röttgering[1], V. Smolčić[7], and F. Walter[8]
[1] Leiden Observatory, Leiden University, P.O. Box 9513, 2300 RA Leiden, The Netherlands; dvdvlugt@strw.leidenuniv.nl
[2] Cosmic Dawn Center (DAWN), Denmark
[3] DTU-Space, Technical University of Denmark, Elektrovej 327, DK-2800 Kgs. Lyngby, Denmark
[4] Hiroshima Astrophysical Science Center, Hiroshima University, 1-3-1 Kagamiyama, Higashi-Hiroshima, Hiroshima 739-8526, Japan
[5] National Astronomical Observatory of Japan, 2-21-1 Osawa, Mitaka, Tokyo, Japan
[6] I. Physikalisches Institut, Universität zu Köln, Zülpicher Strasse 77, D-50937 Köln, Germany
[7] Department of Physics, University of Zagreb, Bijenička cesta 32, 10002 Zagreb, Croatia
[8] Max-Planck-Institut für Astronomie, Königstuhl 17, D-69117 Heidelberg, Germany
Received 2023 January 16; revised 2023 May 12; accepted 2023 May 12; published 2023 July 10

Abstract

Attempts to trace star formation with rest-frame UV/optical observations at redshifts $z > 2$ are affected by the presence of potentially substantial, yet uncertain, dust attenuation. Recent studies have demonstrated the existence of a population of galaxies that are virtually invisible in the observed optical/near-infrared (NIR) due to dust obscuration, but which could contribute substantially to the star formation history at $2 < z < 6$. Here, we make use of ultradeep 3 GHz Karl G. Jansky Very Large Array observations from the COSMOS-XS survey to investigate the contribution 20of radio-selected "optically dark" galaxies (undetected to a depth of $K_S \sim 25.9$ mag) to the cosmic star formation rate density (SFRD). We identify 19 such "optically dark" sources and utilize recent deblended far-infrared photometry to determine photometric redshifts based on IR and radio information for 11 of them. Through stacking, we infer that the remaining eight sources reside predominantly at high redshift ($z > 4$). Therefore, we conservatively assume these sources lie between $z = 2$ and $z = 5$. We derive the radio luminosity function (LF) for the sample with and without "optically dark" sources by fixing the faint and bright end shape of the radio LF to the local values and allowing for luminosity evolution. By integrating both LFs, we estimate the contribution of the "optically dark" galaxies to the radio SFRD to be $\sim 15^{+7}_{-7}\%$ at $z \sim 5$. This is consistent with constraints from NIR-dark and UV-dark sources, while being in disagreement with some estimates using *H*-dropouts. This result implies that "optically dark" sources play a nonnegligible role at high redshift.

Unified Astronomy Thesaurus concepts: Galaxy evolution (594); Star formation (1569); Radio continuum emission (1340)

1. Introduction

For the last 20 yr, pioneering work in the optical/UV has continued to push the frontier of our knowledge of galaxy evolution to higher and higher redshift. Deep surveys with the Hubble Space Telescope (HST) and the development of color selection techniques (e.g., Lyman-break galaxies (LBGs); Steidel et al. 1996) allowed for measurements of the cosmic star formation rate density (SFRD) well beyond the era of peak galaxy assembly ($1 \lesssim z \lesssim 3$) and even into the epoch of reionization (e.g., Bouwens et al. 2020). However, rest-frame optical/UV observations only accurately constrain dust-unobscured star formation, potentially biasing such studies against galaxies with significant dust obscuration (e.g., Madau & Dickinson 2014).

The contribution of galaxies without observable rest-frame optical/UV emission—the "optically dark" population—remains unconstrained by such observations. Samples of optical and near-infrared (NIR)-dark sources have been detected by observing deep CO line emissions (Riechers et al. 2020) and via high angular resolution Atacama Large Millimeter/submillimeter Array (ALMA) studies (e.g., Simpson et al. 2014; Franco et al. 2018; Dudzevičiūtė et al. 2020; Gruppioni et al. 2020; Gómez-Guijarro et al. 2022; Shu et al. 2022; Xiao et al. 2023), suggesting that the classically single-dish-selected submillimeter galaxies (SMGs) that have long been known to be "optically dark" based on pre-ALMA-era observations (e.g., Downes et al. 1999; Smail et al. 1999; Frayer et al. 2004) may be the tip of the iceberg. Most recently, several studies have observed this elusive population with the James Webb Space Telescope (JWST; Barrufet et al. 2023; Pérez-González et al. 2023).

Current simulations underpredict the number density of "optically dark" sources (e.g., Wang et al. 2019). However, different observational studies have also reached varying conclusions about the relative contribution of the "optically dark" population to the cosmic SFRD. While Wang et al. (2019) find that ALMA-observed *H*-dropouts correspond to $\sim 10\%$ of the SFRD from LBGs at similar redshifts ($3 < z < 6$), Talia et al. (2021) report a contribution of $\sim$10%–25% at $z \sim 3.8$ to the UV-SFRD for their sample of radio-selected "optically dark" galaxies, rising to $\sim$25%–40% at $z > 4.5$. Meanwhile, Gruppioni et al. (2020) report that the contribution of their HST+NIR dark sample of galaxies is nearly equal to the total extinction-corrected contribution from all of the known UV-selected galaxies at $z \sim 5$.

Radio observations have been shown to identify "optically dark" galaxies that contribute most significantly to the cosmic SFRD (Talia et al. 2021; Enia et al. 2022). Radio synchrotron emission provides a complementary way to trace star formation owing to its insensitivity to dust obscuration and strong correlation with far-infrared (FIR) emission and star formation rate (SFR) (FIR–radio correlation; e.g., Helou et al. 1985; Delvecchio et al. 2021), although it lacks the benefit of the negative K-correction in the FIR/submillimeter. Recently, the COSMOS-XS survey has been carried out in the COSMOS field over an area of $\sim$350 arcmin^2 at 3 GHz (van der Vlugt et al. 2021, hereafter Paper I). This ultradeep, multiband radio survey has been matched with the extensive multiwavelength data in the COSMOS field (Algera et al. 2020, hereafter Paper II), providing redshift information and enabling improved constraints on the radio-derived SFRD (van der Vlugt et al. 2022, hereafter Paper III). This matching has also revealed a population of radio-detected "optically dark" sources (Paper II), which are likely to be at high redshift ($z > 3$). This sample offers the possibility to study the "optically dark" population uncovered in this ultradeep radio survey and derive the impact on the cosmic SFRD.

Throughout this paper, the spectral index, α, is defined as $S_\nu \propto \nu^\alpha$, where S_ν is the source flux density, and ν is the observing frequency. We use a ΛCDM cosmology with parameters $H_0 = 70\,\mathrm{km\,s^{-1}\,Mpc^{-1}}$, $\Omega_m = 0.3$, and $\Omega_\Lambda = 0.7$ (Bennett et al. 2013). We assume a radio spectral index of -0.7 unless otherwise stated. We assume the Chabrier (2003) initial mass function to calculate SFRs.

2. Data and Sample Selection

In this work, we focus on the radio-selected sample in the COSMOS field obtained from the COSMOS-XS survey.

2.1. COSMOS-XS

The COSMOS-XS survey consists of two overlapping ultradeep single VLA pointings in the COSMOS field at 3 and 10 GHz, respectively. Further details on these observations can be found in Paper I. Summarizing briefly, the 3 and 10 GHz observations reach a depth of 0.53 μJy beam^{-1} and 0.41 μJy beam^{-1} at their respective pointing centers. Both maps have a near-equal resolution of $\sim$2.″0(2.″14 × 1.″81 at 3 GHz and 2.″33 × 2.″01 at 10 GHz).

2.2. Counterparts and Sample Selection

The method to crossmatch the radio sources from the COSMOS-XS survey with their counterparts is fully described in Paper II. We have updated the method slightly, as summarized below (and see the flowchart in Figure 1). We start by taking the 1540 COSMOS-XS 3 GHz sources detected at $\geqslant 5\sigma$ and matching them with the super-deblended photometric catalog (Jin et al. 2018). We then match the resulting catalog with the latest $z^{++}YJHK_s$-selected catalog compiled by Weaver et al. (2022, hereafter COSMOS2020). For sources with multiple redshift estimates, we prioritize spectroscopic redshifts obtained from the COSMOS master catalog (M. Salvato et al. 2023, private communication). For sources without spectroscopic redshifts, we prioritize the photometric redshift from the super-deblended catalog, followed by the photometric redshift from COSMOS2020 or the i-band-selected catalog (Capak et al. 2007) (in that order). However,

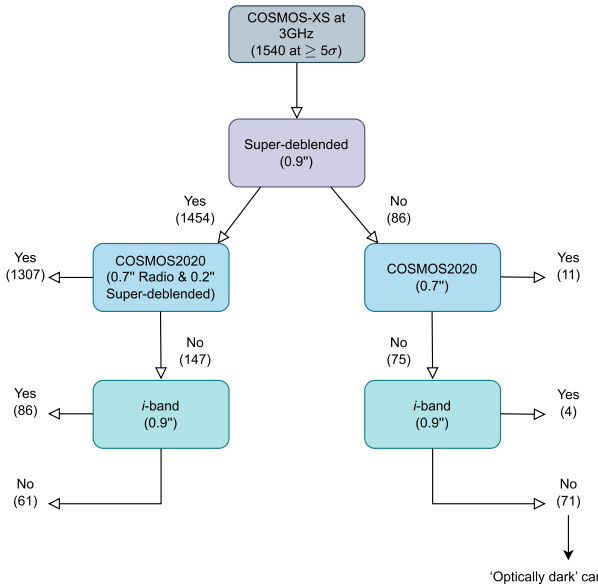

Figure 1. Flowchart of the multiwavelength counterpart-matching process used to identify "optically dark" sources, with numbers of sources and matching radii shown in parentheses. In total, we find 71 sources without counterparts in the optical or NIR catalogs. These sources form the basis of this work.

if a source could be matched within 1.″4 to an X-ray source, the photometric redshift from the Chandra X-ray catalog was used (Civano et al. 2016) because these redshifts have been determined through spectral energy distribution (SED) fitting with the inclusion of active galactic nucleus (AGN) templates. The COSMOS-XS survey has 1408 sources that could be matched to a counterpart in at least one multiwavelength catalog. The number of radio sources with spectroscopic redshifts is 584.

We select the star-forming galaxies (SFGs) from the COSMOS-XS survey, as discussed in Paper III, using the FIR–radio correlation determined by Delvecchio et al. (2021; $q_{\mathrm{TIR}}(M_\star, z)$). As this relation includes stellar mass, we used the mass given by COSMOS2020 for the sources that could be matched with this catalog. For sources without a mass, we used the derived mean mass per redshift bin, ranging from $10^{10.31}\,M_\odot$ to $10^{10.64}\,M_\odot$. When the $q_{\mathrm{TIR}}(M_\star, z)$ of a source deviates by more than 3.0σ from the relation, it is defined as a radio-excess source. This criterion identifies 153 radio-excess sources in total, which are removed from the SFG sample. In addition, following Papers II and III, we remove 62 "inverse radio-excess" sources from the COSMOS-XS survey (of which only 16 were not already identified).

2.3. "Optically Dark" Sources

We find 71 "optically dark" source candidates with no counterpart in the optical or NIR catalogs (5% of the whole COSMOS-XS sample; Figure 1). Based on a similar analysis from Paper II, we expect only $\sim$20 may be spurious radio sources. From these 71 "optically dark" source candidates, a "robust" subsample was compiled by removing sources meeting any of the following criteria: (1) a signal-to-noise ratio (S/N) below 6 at 3 GHz; (2) located near a bright radio source; (3) located near a bright optical/NIR source. The first two criteria are adopted to remove potential spurious radio sources, the last criterion ensures we do not add sources with potential optical counterparts. This results in a sample of 19

Table 1
"Optically Dark" Sources with Their Super-deblended Redshifts

R.A.	Decl.	Total Flux Density at 3 GHz (μJy)	S/N_{FIR}[a]	Redshift[b]
$10^h00^m04^s.8463$	$2^d35^m59^s.5056$	6.21 ± 0.85	4.50	3.50 ± 0.87[c]
$10^h00^m05^s.4573$	$2^d30^m03^s.7998$	5.53 ± 0.89	5.92	4.10 ± 2.00
$10^h00^m07^s.3881$	$2^d42^m03^s.2196$	59.45 ± 3.69	3.52	3.50 ± 0.87[c]
$10^h00^m08^s.6347$	$2^d32^m50^s.8604$	4.50 ± 0.68	0.45	3.50 ± 0.87[c]
$10^h00^m10^s.5157$	$2^d39^m24^s.9492$	21.08 ± 1.48	1.53	3.50 ± 0.87[c]
$10^h00^m14^s.6954$	$2^d28^m01^s.7486$	5.69 ± 0.91	7.33	6.75 ± 3.05[d]
$10^h00^m17^s.1643$	$2^d25^m19^s.1251$	12.53 ± 1.34	6.48	3.50 ± 0.85
$10^h00^m24^s.0435$	$2^d29^m48^s.5492$	6.47 ± 0.61	7.64	4.82 ± 0.00[e]
$10^h00^m24^s.4352$	$2^d37^m49^s.3438$	6.77 ± 0.74	5.24	2.40 ± 1.00
$10^h00^m24^s.5641$	$2^d39^m11^s.5684$	6.34 ± 0.97	10.55	3.00 ± 0.70
$10^h00^m25^s.3726$	$2^d26^m05^s.3135$	7.59 ± 1.05	10.24	4.62 ± 0.00
$10^h00^m28^s.9934$	$2^d29^m37^s.5088$	6.35 ± 0.63	3.85	4.55 ± 0.52
$10^h00^m35^s.3442$	$2^d28^m26^s.6779$	5.83 ± 0.77	19.42	8.55 ± 1.35[f]
$10^h00^m37^s.2974$	$2^d30^m39^s.9243$	4.09 ± 0.65	1.08	3.50 ± 0.87[c]
$10^h00^m38^s.999$	$2^d30^m40^s.1547$	29.37 ± 0.94	0.64	3.50 ± 0.87[c]
$10^h00^m39^s.2093$	$2^d40^m52^s.7322$	27.73 ± 2.20	18.57	3.50 ± 0.70
$10^h00^m48^s.4633$	$2^d36^m41^s.2455$	6.54 ± 1.01	3.03	3.50 ± 0.87[c]
$10^h00^m48^s.7159$	$2^d30^m17^s.9943$	11.54 ± 0.94	9.71	2.90 ± 0.85
$10^h00^m58^s.2531$	$2^d32^m45^s.7583$	8.66 ± 1.36	1.34	3.50 ± 0.87[c]

Notes.
[a] The FIR+mm combined S/N_{FIR} as described in Equation (2) from Liu et al. (2018).
[b] The spectroscopic/photometric/FIR redshift and uncertainty based on SED fitting. An uncertainty of zero refers to a spectroscopic redshift.
[c] This redshift is sampled from a uniform distribution between $z = 2$ and $z = 5$ because $S/N_{FIR} < 5$. The redshift given here is the median of the distribution and the error is the standard deviation of the distribution.
[d] Removed from the "optically dark" sample by the cut on $q_{TIR}(M_\star, z)$.
[e] Spectroscopic redshift from recent ALMA observations as determined by N. B. Sillassen et al. (in preparation).
[f] This promising candidate at $z > 6 - 9$ is a target in an ongoing NOEMA line scan project.

robust "optically dark" sources invisible to a depth of $K_S \sim 25.9$ mag (none of which have a counterpart in the Chandra X-ray catalog). Previously, Paper II reported the discovery of 70 "optically dark" source candidates with no counterpart in the optical or NIR catalogs, with the main difference being the use of the COSMOS2015 catalog. They found 29 robust sources using the outlined criteria above.

By adding the COSMOS-XS sources to a prior catalog based on the COSMOS2020 catalog (Weaver et al. 2022), we adopted the "super-deblending" technique (Jin et al. 2018; Liu et al. 2018) and deblended FIR/(sub)millimeter to radio data in COSMOS-XS on the priors' positions. For the 19 robust "optically dark" sources in the new super-deblended catalog in COSMOS (S. Jin et al. 2023, in preparation), we have deblended photometry in MIPS 24 μm, Herschel, SCUBA2, AzTEC, MAMBO, VLA 1.4 and 3 GHz, and MeerKAT 1.28 GHz band, in which 11 of them are detected in FIR with combined $S/N_{FIR} > 5$, providing FIR–luminosity (L_{FIR}) values. In total, 2/19 sources have a spectroscopic redshift from the COSMOS master catalog. For the $S/N_{FIR} > 5$ sources without spectroscopic redshifts, we then used the FIR-based photometric redshifts based on the method described in Jin et al. (2018) and briefly summarized below. Four distinct SED components are used in the fitting procedure: (1) a stellar component (Bruzual & Charlot 2003) with a Small Magellanic Cloud dust attenuation law; (2) a mid-infrared (MIR) AGN torus component (Mullaney et al. 2011); (3) dust continuum emission from the Magdis et al. (2012) library with the more updated L_{IR}/M_{dust}-redshift evolution taken from Béthermin et al. (2015); and (4) a power-law radio continuum with an evolving q_{TIR}. Examples of the SED fits and multiwavelength cutouts of $z > 4$ candidates can be found in Figure 23 of Jin et al. (2018), and two of these candidates have weak or no detection in the K_S band similar to the "optically dark" sources. Jin et al. (2018) note that the IR SED-driven photometric redshifts of $z > 3$ are in good agreement with the spectroscopic redshift for galaxies with significant FIR detections, while it is somewhat underestimated for galaxies with significant AGN torus emission. We find that the FIR-based photometric redshifts for the two "optically dark" sources found within the spectroscopic COSMOS master catalog agree with their spectroscopic redshift within 1σ uncertainty. Additionally, recent ALMA spectral scans of a similarly selected population find that 7/9 sources with lines detected have spectroscopic redshifts that agree with their FIR photometric redshifts within $<2\sigma$ (project 2022.1.00863.S, PI: Hodge). Despite the dispersion, the spectroscopic redshifts confirm that all of the "optically dark" sources targeted are at $z \gtrsim 3$, as suggested by their estimated FIR photometric redshifts.

Finally, for the 8/19 sources with $S/N_{FIR} < 5$, we estimated the redshift probability distribution from the stacking analysis as described in Section 5.3 in Paper II. The final SED and redshift probability distribution showed that a sample of "optically dark" sources without counterparts predominantly consists of high-redshift ($z > 4$) sources, as can be seen in Figure 15 in Paper II. The eight sources are thus added to the "optically dark" sample with a redshift conservatively sampled from a uniform distribution between $z = 2$ and $z = 5$.

The properties of the 19 robust "optically dark" sources are listed in Table 1, and the redshift and total flux density distributions are shown in Figure 2 compared to the redshift and total flux density distribution of the COSMOS-XS sample.

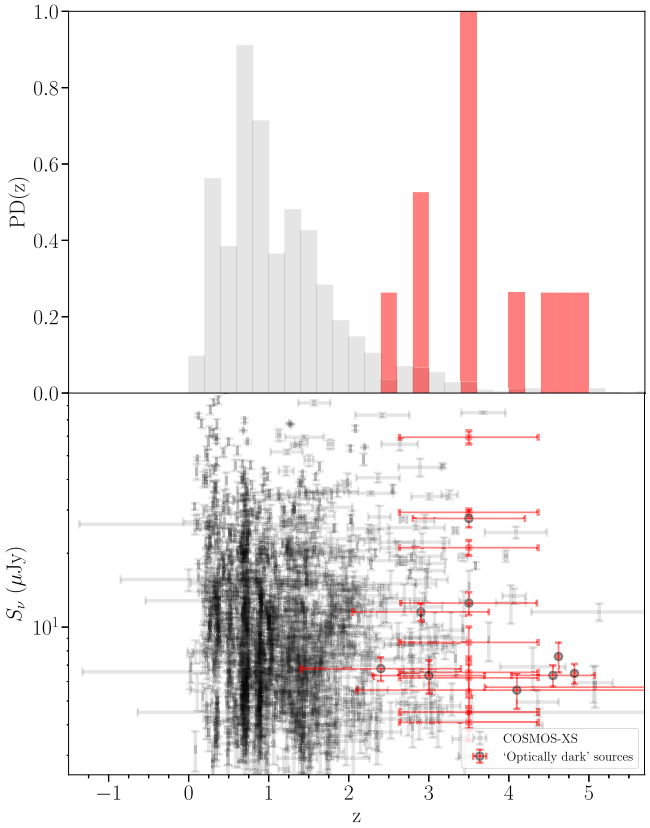

Figure 2. The upper panel shows a histogram of the redshift distribution of the COSMOS-XS sample compared to the 19 "optically dark" sources. All but one of these sources are found to be SFGs. The lower panel shows the total flux density vs. redshift distributions of the COSMOS-XS sample compared to the "optically dark" sources. In total, ∼68% of the "optically dark" sources fall below 10 μJy. The FIR-based photometric redshifts of the "optically dark" population are found using SED fitting on the new super-deblended photometry. The sources without a black edge consist of the sample of eight "optically dark" sources with an FIR detection of $S/N_{FIR} < 5$. The error bar of these sources represents the standard deviation of the distribution. Their redshift is sampled from a uniform distribution between $z = 2$ and $z = 5$.

In addition, Table 2 shows the number of "optically dark" sources+nondark sources in the four bins compared to the nondark sources in the bin. The four bins range from $z = 2$ to $z = 5.7$, and we note that changing the bins does not change our results. We find that the "optically dark" sample makes up $\sim 12\%$ of the total number of sources at $z > 2$. The derived redshift distribution confirms that the bulk of our population of "optically dark" sources consists of dusty SFGs at $z > 2$. However, we note that the photometric redshifts contain a large photometric error, with a typical uncertainty of 0.85. The total flux density distribution in Figure 2 shows that ∼68% of the "optically dark" sources fall below 10 μJy.

Lastly, we select SFGs from the 19 "optically dark" sources with $S/N_{FIR} > 5$ using the FIR–radio correlation as discussed above (and we also note that the fraction of COSMOS-XS radio sources powered by star formation in general already reaches near-unity below 20 μJy (Paper II)). One of the 19 sources is removed by the cut on $q_{TIR}(M_\star, z)$, where the mass is the derived mean mass per redshift bin and L_{FIR} is found in the super-deblended FIR catalog. This leaves 18 "optically dark" sources that are classified as SFGs. This sample will be used to estimate the contribution of the "optically dark" galaxies to the radio SFRD.

3. Contribution of the "Optically Dark" Population to the SFRD

We measure the impact of "optically dark" sources by constructing the radio luminosity function (LF) with and without these sources. Using these radio LFs, we then derive the SFRD and quantify the contribution of the "optically dark" sources to the radio SFRD.

3.1. Constraining the LF

The radio LFs are derived using the same $1/V_{max}$ (Schmidt 1968) method as described in Paper III. We will briefly summarize the method below.

In each redshift bin, we compute the comoving volume available to each source in that bin. Following Paper III, this volume is corrected with the completeness correction factor, which takes into account the observed area and sensitivity limit. However, we do not correct for counterpart completeness in this work given that we are interested in exactly those sources with no optical/NIR counterparts. We use the parametric estimate of the LF at different redshifts as done in Paper III to fit the LF. We assume a modified Schechter function (e.g., Saunders et al. 1990) for the shape of the LF, where the values of $\Phi_\star$, α, and σ will be frozen at the values found for the local LF. In reality, $\Phi_\star$, α, and σ may change with redshift. We use the parameters of the local LF as determined in Paper III. When we fit the LF, we only assume the position of the turnover ($L_\star$, characteristic luminosity) to change with the redshift. The reason is we are not able to constrain both $L_\star$ and $\Phi_\star$ for the higher redshifts ($z > 2.0$). All sources are distributed into equally spaced luminosity bins spanning the observed luminosity range. The LFs calculated with the V_{max} method are shown in Figure 3. The LFs are calculated using the 1.4 GHz rest-frame luminosity for easier comparison with previous studies.

In order to take the uncertainties on the photometric redshifts into account, we measure the luminosity function for 1000 different realizations of z and $\log L$, extracted from their probability density distributions. The distributions are taken to be Gaussian. The error is defined as the 16th and 84th percentiles of the final distribution added to the median error, as calculated with Equation (6) in Paper III in quadrature.

The black filled circles show the median luminosity of all sources, including the "optically dark" sources, in the corresponding luminosity bin. The black open circles are a reference as they consist of the COSMOS-XS data set without "optically dark" sources. The horizontal error bars show the width of the bin. The vertical errors correspond to the errors calculated using Equation (6) in Paper III. The data points were fitted with the analytical form from Equation (1) using the Markov Chain Monte Carlo algorithm assuming flat priors[9]:

$$\Phi(L, z, \alpha_L) = \Phi_0\left(\frac{L}{(1+z)^{\alpha_L}}\right), \quad (1)$$

where α_L corresponds to the pure evolution parameter and Φ_0 is given in Equation (7) in Paper III.

The redshift used in Equation (1) is the median redshift of all of the sources in the redshift bin. This value is given in the panels of Figure 3. The best-fit values for α_L are tabulated in

[9] $\alpha_L \in [1.0, 7.0]$.

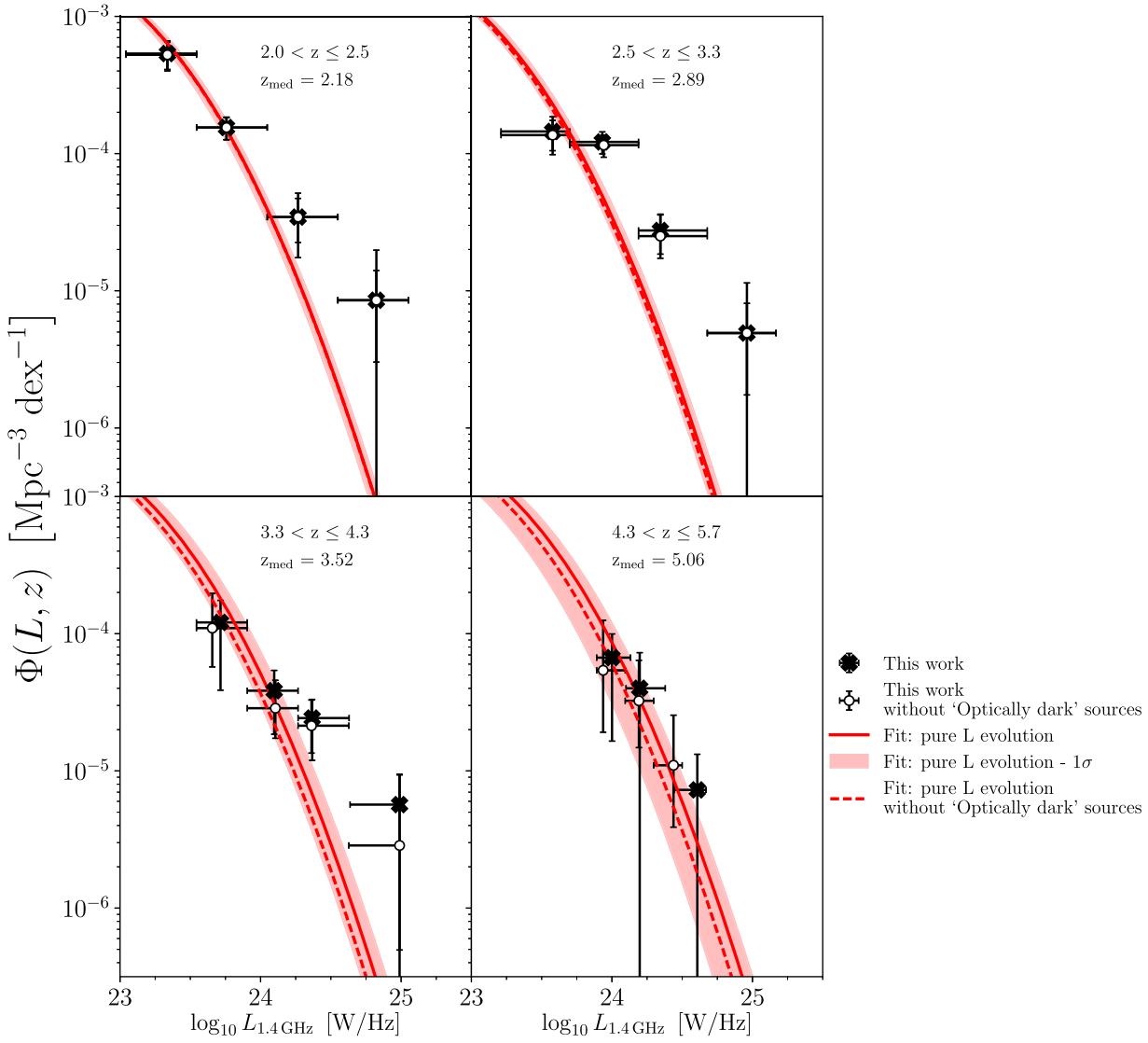

Figure 3. Radio LFs of SFGs in four redshift bins from the COSMOS-XS survey. Our best-fit pure luminosity function, fitted to the black points, in each redshift bin is shown with solid red, where the shaded area shows the 1σ confidence interval for the best-fit function. The dotted red line is the best-fit pure luminosity function fitted to the open symbols. The redshift range and median redshift are given in each panel. The open symbols show the LF without the contribution of "optically dark" sources and the filled symbols show the LF including "optically dark" sources. The difference between the open and filled symbols shows the impact of the contribution of the "optically dark" sources, which is especially notable in the highest-redshift bin.

Table 2
Parameter Values Describing the Luminosity Evolution Fits to the COSMOS-XS Data Set and to the COSMOX-XS Data Set + "Optically Dark" Sources

Redshift Range	Median Redshift	COSMOS-XS			COSMOS-XS + "Optically Dark" Sources		
		α_L	Number of Sources	SFRD[a] ($M_\odot$ yr^{-1} Mpc^{-3})	α_L	Number of Sources	SFRD[a] ($M_\odot$ yr^{-1} Mpc^{-3})
$2.0 < z < 2.5$	2.18	$2.20^{+0.08}_{-0.09}$	69	$0.075^{+0.009}_{-0.009}$	$2.21^{+0.08}_{-0.08}$	70	$0.075^{+0.010}_{-0.009}$
$2.5 < z < 3.3$	2.89	$1.72^{+0.07}_{-0.09}$	58	$0.057^{+0.008}_{-0.007}$	$1.76^{+0.07}_{-0.08}$	60	$0.059^{+0.009}_{-0.008}$
$3.3 < z < 4.6$	3.52	$1.60^{+0.13}_{-0.19}$	18	$0.056^{+0.013}_{-0.015}$	$1.70^{+0.11}_{-0.16}$	29	$0.065^{+0.014}_{-0.015}$
$4.6 < z < 5.7$	5.06	$1.47^{+0.15}_{-0.21}$	7	$0.071^{+0.023}_{-0.023}$	$1.57^{+0.14}_{-0.23}$	10	$0.082^{+0.026}_{-0.029}$

Note.
[a] Obtained by integrating the fitted LF from $L_{\rm min} = 0.0$ to $L_{\rm max} = \infty$.

Table 2 and the best-fit pure luminosity evolved function is shown with the red line in Figure 3. The difference between the open and filled symbols shows the impact of the contribution of the "optically dark" sources, which is especially notable in the highest-redshift bin.

3.2. SFRD

The radio SFRD is derived using the same method as described in Paper III. We will briefly summarize the method below. The SFRD is estimated by taking the luminosity-

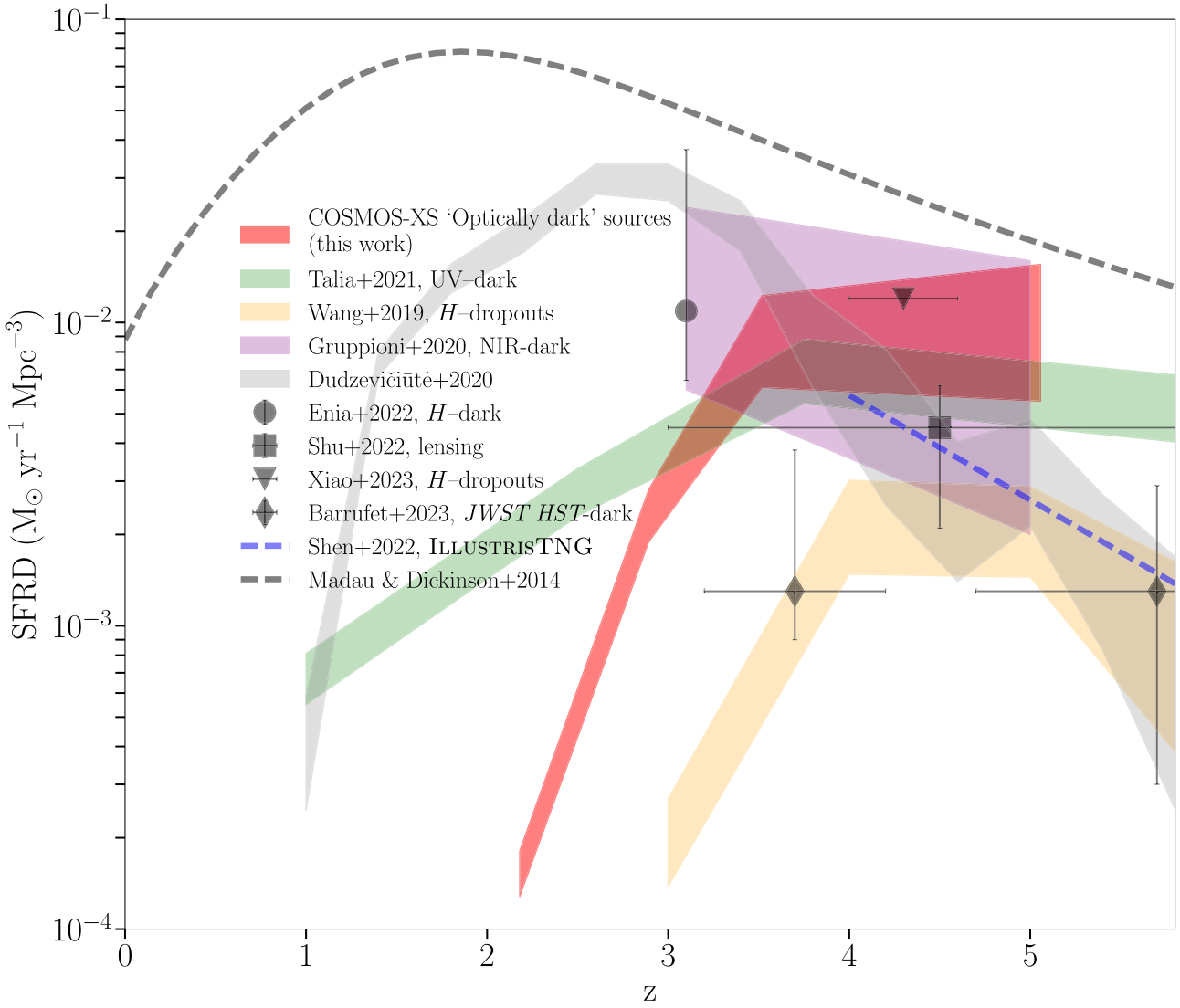

Figure 4. The cosmic star formation rate density history. The black dotted curve represents the study of Madau & Dickinson (2014). The red shaded area shows the 1σ confidence interval for the contribution of "optically dark" COSMOS-XS sources to the SFRD. The green area and the black point show the SFRD from radio-selected UV-dark galaxies from Talia et al. (2021) and Enia et al. (2022), respectively. The yellow area is the SFRD from the *H*-dropouts in Wang et al. (2019) and the purple region shows the subsample of NIR-dark galaxies in the ALPINE fields (Gruppioni et al. 2020). The black square, triangle, and diamond give the SFRD from the recent studies by, respectively, Shu et al. (2022), Xiao et al. (2023), and Barrufet et al. (2023). The blue dashed line shows the results from the IllustrisTNG simulations (Shen et al. 2022). The gray area shows, for reference, the SMG contribution for a complete dust-mass-selected sample to the SFRD from Dudzevičiūtė et al. (2020). Our estimate of the "optically dark" contribution stays constant for $3.5 \lesssim z \lesssim 5.0$ and the "optically dark" sources contribute $\sim 15^{+7}_{-7}\%$ of the total radio-derived SFRD at $z \sim 5$.

weighted integral of the analytical form of the fitted LF and converting the luminosity in the integral to SFR. The integral of the SFRD is given by Equation (16) in Paper III. This integral gives the SFRD of a given epoch. The results of the SFRD shown in Figure 4 are obtained by integrating the fitted LF from 0.0 to $\rightarrow \infty$. Our errors are estimated from the fitting parameter uncertainties through bootstrapping, whereby the uncertainties in $q_{\rm TIR}(M_\star, z)$ are taken into account. The error is defined as the 16th and 84th percentiles of the final distribution. The quoted errors do not account for any systematic errors due to cosmic variance. The total SFRD for the COSMOS-XS sample and the COSMOS-XS sample including "optically dark" sources are shown in Table 2. We find that at $z \sim 2.9$ "optically dark" sources account for $\sim 2^{+0.4}_{-0.4}\%$ of the total radio SFRD derived from the full radio sample. This fraction rises with redshift until $z \sim 3.5$, reaching $\sim 17^{+5}_{-6}\%$ at $z \sim 3.5$ and $\sim 15^{+7}_{-7}\%$ at $z \sim 5.1$. Their contribution to the SFRD is shown in Figure 4. As the radio observations do not constrain the location of the knee and the faint-end slope, we have also integrated the LF using the luminosity limit reached by the radio observations in the range $z = 2.0$ and $z = 2.5$, which is $\log_{10} L_{1.4\,\rm GHz} = 23.0\,\rm W\,Hz^{-1}$. This does not change the results significantly and we find at $z \sim 2.9$ a contribution of $\sim 0.3^{+0.3}_{-0.3}\%$, reaching $\sim 33^{+16}_{-17}\%$ at $z \sim 3.5$ and $\sim 21^{+14}_{-14}\%$ at $z \sim 5.1$. The sky density of star-forming "optically dark" sources is approximately $185 \pm 44\,\rm deg^{-2}$. This is within the error of the potential surface density found by Smail et al. (2021) of $450^{+750}_{-300}\,\rm deg^{-2}$ for NIR-faint SMGs. It is lower than the ALMA-selected *H*-dropout surface density corrected for incompleteness of $530\,\rm deg^{-2}$ (Wang et al. 2019).

Table 3
Criteria for "Optically Dark" Sources

Study	Definition "Optically Dark"	$L_{1.4}$ GHz at z = 4 Limit (W Hz^{-1})	SFRD at $z = 4$ ($M_\odot$ yr^{-1} Mpc^{-3})
Our study	No counterpart in COSMOS2020 and super-deblended ($K_S = 25.9$ mag)	4.29×10^{23}	$0.010^{+0.013}_{-0.006}$
Talia et al. (2021)	No counterpart in NIR-to-FIR bands ($K_S = 24.5 - 24.9$ mag)	1.86×10^{24}	0.007 ± 0.002
Wang et al. (2019)	No counterpart in the H-band ($H > 27$ mag, [4.5] < 24 mag)	6.28×10^{23}[a]	0.002 ± 0.007
Gruppioni et al. (2020)	No counterpart in HST or NIR ($K_S = 24.9$ mag)	8.31×10^{22}[a]	0.01 ± 0.008
Enia et al. (2022)	No counterpart in HST/WFC3 H-band ($H = 27.3$ mag)	1.04×10^{24}	0.01 ± 0.004[b]
Jin et al. (2022)	No counterpart in ($K_S = 24.9$ mag)	6.28×10^{23}[a]	0.0026
Xiao et al. (2023)	No counterpart in HST/WFC3 H-band ($H > 26.5$ mag) and IRAC ([4.5] = 25 mag)	9.53×10^{23}	0.012[c]
Barrufet et al. (2023)	HST-dark galaxies selected on $H - F444W$ colors ($H - F444W > 2.3$, $H > 27$ mag, $F444W > 26.4$ mag)	2.05×10^{22}[a]	$0.0013^{+0.0024}_{-0.0005}$
Shu et al. (2022)	No counterpart in HST/WFC3 H-band ($H > 27.5$ mag)	9.60×10^{22}[a]	$0.0045^{+0.0017}_{-0.0024}$[d]

Notes.
[a] Converted to radio luminosity at 1.4 GHz using the FIR–radio correlation determined by Delvecchio et al. (2021). As this relation includes stellar mass, we use the mean mass at $z = 4$ found for the COSMOS-XS sample ($10^{10.41}$ $M_\odot$).
[b] SFRD at $z = 3$ since Enia et al. (2022) do not derive the SFRD at $z = 4$.
[c] SFRD at $z = 4.3$ since Xiao et al. (2023) do not derive the SFRD at $z = 4$.
[d] SFRD at $z = 4.5$ since Shu et al. (2022) do not derive the SFRD at $z = 4$.

3.3. Discussion

Different works have already identified "optically dark" sources, extreme SFGs heavily obscured by dust that lack an optical or NIR counterpart, out to high redshift ($z \simeq 5$; e.g., Simpson et al. 2014; Wang et al. 2019; Dudzevičiūtė et al. 2020; Gruppioni et al. 2020; Talia et al. 2021; Enia et al. 2022; Shen et al. 2022). Figure 4 shows the results from a number of recent observational and theoretical studies compared to this work. The definitions and depths of the observational studies are listed in Table 3. For reference, Figure 4 also shows the SMG contribution for a complete dust-mass-selected sample to the SFRD from Dudzevičiūtė et al. (2020).

Most observational studies show that the contribution of "optically dark" sources increases up to $z \sim 3.5$ and thereafter decreases. However, the observations still span a wide range of SFRD values over 1 order of magnitude at $3 \lesssim z \lesssim 6$. Part of the difference among observational studies could be due to the different selection criteria for these various optical and NIR-"dark" samples, leading Talia et al. (2021) to suggest a possible diversity of galaxy populations under the common "dark" label. Figure 4 includes two other studies of radio-selected "optically dark" galaxies: Talia et al. (2021) used radio sources without counterparts in the COSMOS2015 catalog (Laigle et al. 2016) and Enia et al. (2022) selected radio galaxies lacking a counterpart in the HST/WFC3 H-band. Figure 4 also shows "optically dark" sources that were selected from Spitzer/IRAC imaging or as serendipitous sources in ALMA submillimeter continuum data. Wang et al. (2019) reported ALMA follow-up observations of a population of H-dropouts, while Shu et al. (2022) reported ALMA and JCMT/SCUBA2 follow-up of 12 strongly lensed galaxies also selected as H-dropouts, and Gruppioni et al. (2020) utilized serendipitous ALMA continuum detections around main-sequence galaxies. Recently, Barrufet et al. (2023) presented a JWST study of HST-dark galaxies, which were selected with similar color cuts to select the H-dropout galaxies. Finally, Xiao et al. (2023) extended the H-dropout criterion, using multi-wavelength observations ranging from HST to ALMA, to select normal star-forming galaxies with lower stellar masses ($\log(M_\star/M_\odot) = 9.5 - 10.5$).

Compared to these non-radio-based studies, our results are most consistent with Gruppioni et al. (2020) and Xiao et al. (2023) at $z \sim 4$, and somewhat higher than the results of Wang et al. (2019), Shu et al. (2022), and Barrufet et al. (2023). This might be due to the selection criteria used in these studies to select the H-dropout population. Xiao et al. (2023) showed that Wang et al. (2019) selected only extremely dust-obscured massive galaxies with a median mass of $\log(M_\star/M_\odot) = 10.6$. Meanwhile, Barrufet et al. (2023) used similar color cuts to Wang et al. (2019) to identify their sample. Studies using radio emission are less likely to be biased toward these extreme objects because of the lack of dependence on dust temperature but are more likely to be biased by radio emission originating from AGN.

Our selection criteria are closest to the studies by Talia et al. (2021) and Enia et al. (2022), as they both used radio surveys to identify their "optically dark" sources. Indeed, we find general agreement with Talia et al. (2021) at $z \sim 3$, though the behavior at lower and higher redshift is somewhat different. The remaining differences between these radio-based observational studies (and their associated uncertainties) could be partly explained by the redshifts assumed for the "optically dark" sources. Talia et al. (2021) estimated redshifts using SED fitting for sources with one FIR and one NIR-to-MIR photometric point from COSMOS2015 and the super-deblended catalogs (comprising ~50% of their sample), and they estimated the photometric distribution for the other sources from a stacked SED. As Enia et al. (2022) did not have redshift constraints for ~50% of their "optically dark" sample, they assumed those sources to be at $z \sim 3$. For the other sources, they estimated their photometric redshift from SED fitting. In this study, we have attempted to mitigate some of this uncertainty by using the latest super-deblended FIR catalog to determine FIR-based photometric redshifts for our individual sources, though we caution that the uncertainties are still significant, as shown in Figure 2. Precise redshifts for the "optically dark" sources would help us to place more robust

constraints on the relative contribution of "optically dark" sources to the SFRD.

A final consideration, at least in observational studies like ours, is the effect of small number statistics and cosmic variance. Our small observed area is likely to suffer from cosmic variance, as was also discussed in Paper III, and might explain some of the discrepancies with other observational studies. Observing larger areas to the depth achieved here would help to place more precise constraints.

Forming dusty galaxies at high redshift in simulations while simultaneously matching constraints from other low- or high-redshift galaxy populations has been surprisingly problematic for theorists (e.g., Casey et al. 2014). To illustrate the difference between observations and simulations, Figure 4 also shows the result from the recent theoretical study by Shen et al. (2022). They used postprocessed galaxies in the ILLUSTRISTNG simulation and find a strongly decreasing trend at $z > 4$, where their predicted obscured SFRD becomes subdominant (i.e., contributes less than 50% to the total SFRD) at $z \gtrsim 5$ and diminishes at higher redshift. This is also an upper limit as they assume that all of the galaxies with $L_{\rm IR} = 10^{12}\,L_{\odot}$ are optical and NIR dark. This discrepancy between the observations and the ILLUSTRISTNG simulation is related to the underprediction of luminous IR galaxies in the model.

4. Summary and Conclusions

We make use of ultradeep 3 GHz Karl G. Jansky Very Large Array observations of the COSMOS field from the multiband COSMOS-XS survey to infer the contribution of "optically dark" sources to the cosmic SFRD. Approximately 5% of all COSMOS-XS radio sources are found to be optically and NIR dark (to a depth $K_S \sim 25.9$ mag). Using redshift estimates either from newly deblended FIR photometry or informed by stacking, we estimate the contribution of these "optically dark" sources to the SFRD by deriving the radio LF for the sample with and without this population.

We identify a robust subsample of 19 "optically dark" sources between $2 < z < 5$ and derive their contribution to the radio SFRD. We conclude that "optically dark" sources contribute $\sim 15^{+7}_{-7}\%$ of the total radio-derived SFRD at $z \sim 5$. In addition, we find the contribution stays constant for $3.5 \lesssim z \lesssim 5.0$. Our derived contribution at $z \sim 5$ is in agreement with some previous observational results from NIR- and UV-dark sources by Gruppioni et al. (2020), Talia et al. (2021), and Xiao et al. (2023), but higher than some estimates based on *H*-dropouts. This result highlights that "optically dark" sources possibly play a nonnegligible role at high redshift. In addition, it shows the advantage of deep radio imaging in observing the "optically dark" population, which will be even more feasible with future deep and wide radio surveys, such as the SKA, ngVLA, and MeerKAT.

Acknowledgments

We wish to thank the anonymous referee for the comments and suggestions, which greatly improved this work. The authors wish to thank Ian Smail for the useful discussions that helped improve this work and Mara Salvato for providing us with the COSMOS spectroscopic master catalog. The National Radio Astronomy Observatory is a facility of the National Science Foundation operated under cooperative agreement by Associated Universities, Inc. D.v.d.V. and J.H. acknowledge the support of the VIDI research program with project No. 639.042.611, which is (partly) financed by the Netherlands Organisation for Scientific Research (NWO). H.S.B.A. acknowledges support from NAOJ ALMA Scientific Research Grant Code 2021-19A. S.J. is supported by the European Union's Horizon Europe research and innovation program under the Marie Skłodowska-Curie grant agreement No. 101060888. This research made use of ASTROPY, a community-developed core Python package for astronomy (Astropy Collaboration et al. 2013, 2018) hosted at http://www.astropy.org/, Matplotlib (Hunter 2007), NumPy (van der Walt et al. 2011), SciPy (Jones et al. 2001), and of TOPCAT (Taylor 2005).

ORCID iDs

J. A. Hodge https://orcid.org/0000-0001-6586-8845
S. Jin https://orcid.org/0000-0002-8412-7951
H. S. B. Algera https://orcid.org/0000-0002-4205-9567
S. K. Leslie https://orcid.org/0000-0002-4826-8642
D. A. Riechers https://orcid.org/0000-0001-9585-1462
H. Röttgering https://orcid.org/0000-0001-8887-2257
V. Smolčić https://orcid.org/0000-0002-3893-8614
F. Walter https://orcid.org/0000-0003-4793-7880

References

Algera, H. S. B., van der Vlugt, D., Hodge, J. A., et al. 2020, ApJ, 903, 139
Astropy Collaboration, Price-Whelan, A. M., Sipőcz, B. M., et al. 2018, AJ, 156, 123
Astropy Collaboration, Robitaille, T. P., Tollerud, E. J., et al. 2013, A&A, 558, A33
Barrufet, L., Oesch, P. A., Weibel, A., et al. 2023, MNRAS, 522, 449
Bennett, C. L., Larson, D., Weiland, J. L., et al. 2013, ApJS, 208, 20
Béthermin, M., Daddi, E., Magdis, G., et al. 2015, A&A, 573, A113
Bouwens, R., González-López, J., Aravena, M., et al. 2020, ApJ, 902, 112
Bruzual, G., & Charlot, S. 2003, MNRAS, 344, 1000
Capak, P., Aussel, H., Ajiki, M., et al. 2007, ApJS, 172, 99
Casey, C. M., Narayanan, D., & Cooray, A. 2014, PhR, 541, 45
Chabrier, G. 2003, PASP, 115, 763
Civano, F., Marchesi, S., Comastri, A., et al. 2016, ApJ, 819, 62
Delvecchio, I., Daddi, E., Sargent, M. T., et al. 2021, A&A, 647, A123
Downes, D., Neri, R., Greve, A., et al. 1999, A&A, 347, 809
Dudzevičiūtė, U., Smail, I., Swinbank, A. M., et al. 2020, MNRAS, 494, 3828
Enia, A., Talia, M., Pozzi, F., et al. 2022, ApJ, 927, 204
Franco, M., Elbaz, D., Béthermin, M., et al. 2018, A&A, 620, A152
Frayer, D. T., Reddy, N. A., Armus, L., et al. 2004, AJ, 127, 728
Gómez-Guijarro, C., Elbaz, D., Xiao, M., et al. 2022, A&A, 658, A43
Gruppioni, C., Béthermin, M., Loiacono, F., et al. 2020, A&A, 643, A8
Helou, G., Soifer, B. T., & Rowan-Robinson, M. 1985, ApJL, 298, L7
Hunter, J. D. 2007, CSE, 9, 90
Jin, S., Daddi, E., Liu, D., et al. 2018, ApJ, 864, 56
Jin, S., Daddi, E., Magdis, G. E., et al. 2022, A&A, 665, A3
Jones, E., Oliphant, T., Peterson, P., et al. 2001, http://www.scipy.org/
Laigle, C., McCracken, H. J., Ilbert, O., et al. 2016, ApJS, 224, 24
Liu, D., Daddi, E., Dickinson, M., et al. 2018, ApJ, 853, 172
Madau, P., & Dickinson, M. 2014, ARA&A, 52, 415
Magdis, G. E., Daddi, E., Béthermin, M., et al. 2012, ApJ, 760, 6
Mullaney, J. R., Alexander, D. M., Goulding, A. D., & Hickox, R. C. 2011, MNRAS, 414, 1082
Pérez-González, P. G., Barro, G., Annunziatella, M., et al. 2023, ApJL, 946, L16
Riechers, D. A., Hodge, J. A., Pavesi, R., et al. 2020, ApJ, 895, 81
Saunders, W., Rowan-Robinson, M., Lawrence, A., et al. 1990, MNRAS, 242, 318
Schmidt, M. 1968, ApJ, 151, 393
Shen, X., Vogelsberger, M., Nelson, D., et al. 2022, MNRAS, 510, 5560
Shu, X., Yang, L., Liu, D., et al. 2022, ApJ, 926, 155
Simpson, J. M., Swinbank, A. M., Smail, I., et al. 2014, ApJ, 788, 125
Smail, I., Dudzevičiūtė, U., Stach, S. M., et al. 2021, MNRAS, 502, 3426
Smail, I., Ivison, R. J., Kneib, J. P., et al. 1999, MNRAS, 308, 1061

Steidel, C. C., Giavalisco, M., Dickinson, M., & Adelberger, K. L. 1996, AJ, 112, 352
Talia, M., Cimatti, A., Giulietti, M., et al. 2021, ApJ, 909, 23
Taylor, M. B. 2005, in ASP Conf. Ser. 347, Astronomical Data Analysis Software and Systems XIV, ed. P. Shopbell, M. Britton, & R. Ebert (San Francisco, CA: ASP), 29
van der Vlugt, D., Algera, H. S. B., Hodge, J. A., et al. 2021, ApJ, 907, 5
van der Vlugt, D., Hodge, J. A., Algera, H. S. B., et al. 2022, ApJ, 941, 10
van der Walt, S., Colbert, S. C., & Varoquaux, G. 2011, CSE, 13, 22
Wang, T., Schreiber, C., Elbaz, D., et al. 2019, Natur, 572, 211
Weaver, J. R., Kauffmann, O. B., Ilbert, O., et al. 2022, ApJS, 258, 11
Xiao, M. Y., Elbaz, D., Gómez-Guijarro, C., et al. 2023, A&A, 672, A18